DOI 10.1007/s10593-023-03175-1

Chemistry of Heterocyclic Compounds **2023**, *59*(3), 138–144

Regio- and stereoselectivity of [3+2] cycloaddition reactions between (*Z*)-1-(anthracen-9-yl)-*N*-methyl nitrone and analogs of *trans*-β-nitrostyrene on the basis of MEDT computational study

Karolina Kula[1]*, Mikołaj Sadowski[1]

[1] *Cracow University of Technology, Institute of Organic Chemistry and Technology, 24 Warszawska St., Cracow PL-31-155, Poland; e-mail: kkula@chemia.pk.edu.pl*

Published in Khimiya Geterotsiklicheskikh Soedinenii, 2023, *59*(3), 138–144

Submitted October 17, 2022
Accepted after revision November 29, 2022

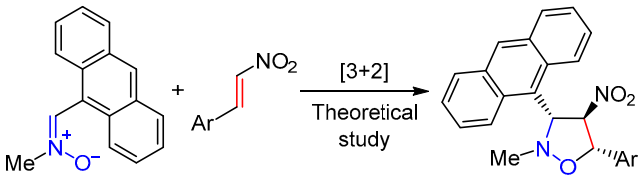

Ar = Ph, 4-$O_2NC_6H_4$, 4-$H_2NC_6H_4$

The regio- and stereoselectivity of [3+2] cycloaddition reactions of (*Z*)-1-(anthracen-9-yl)-*N*-methyl nitrone with analogs of *trans*-β-nitrostyrene were studied within the molecular electron density theory at the B3LYP/6-31G(d) and MPWB95/6-311G(d,p) theory levels. Analysis of the reactivity indices for presented reactions suggests that nitrone participates as nucleophile, while studied nitroalkenes play a role of electrophiles. According to electron localization function and conceptual density functional theory, kinetic and thermodynamic aspects of processes as well as analysis of all critical structures, the most favored reaction path is the formation of (3*RS*,4*RS*,5*SR*)-3-(anthracen-9-yl)-5-aryl-2-methyl-4-nitroisoxazolidine, independently of simulated solvent.

Keywords: nitrone, β-nitrostyrene, cycloaddition reaction, molecular electron density theory, molecular mechanism.

Isoxazolidines are a group of five-membered, saturated heterocyclic compounds containing both nitrogen and oxygen in the skeleton.[1] This class of compounds, due to their biological activity, found use in many aspects of life.[2] Isoxazolidines are widely used in medicine as antibacterial and antiviral drugs.[3,4] An example to be mentioned is cycloserine which is a common structural motif in antibiotics[5] (Fig. 1). Besides, isoxazolidines are used in industry as a part of scrubbers to remove sulfur-containing compounds[6] or in polymer chemistry as a part of copolymers.[7]

The most universal and common protocols for the synthesis of isoxazolidines and their derivatives, comprise [3+2] cycloaddition (32CA) reactions of nitrones with olefins,[8–10] proceeding under mild conditions in absence of catalyst and giving high yields.[11,12] This method also allows to obtain products with high or complete selectivity.[13,14] Moreover, 32CA reactions are characterized by complete atom economy. The full atom economy of the above processes lies in accordance with green chemistry rules.[15,16]

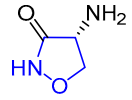

Figure 1. Structure of cycloserine (4-amino-3-isoxazolidinone).

In our research, the study on possibility of synthesis of sterically crowded *N*-methylisoxazolidines was carried out (Scheme 1). In order to achieve assumed purpose, (*Z*)-1-(anthracen-9-yl)-*N*-methyl nitrone (**1**) was applied as a three-atom component (TAC).[17] Nitrone **1** has already been tested in 32CA reaction giving high yields of

Scheme 1

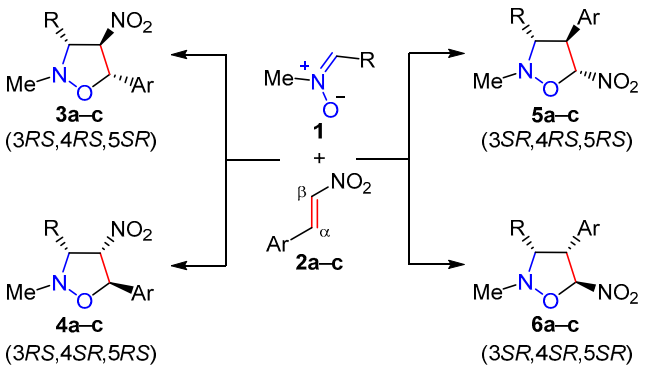

R = anthracen-9-yl; **a** Ar = 4-$H_2NC_6H_4$, **b** Ar = Ph, **c** Ar = 4-$O_2NC_6H_4$

products.[3] Simultaneously, the protocol of synthesis of nitrone **1** is not complicated and according to the literature, the molecule possesses biological activity.[18] In turn, the series of *trans*-β-nitrostyrene analogs **2a–c** were used as alkenes. It is well known, that conjugated nitroalkenes are commonly used in 32CA reactions.[19,20] Moreover, as *in vitro* tests show, *trans*-β-nitrostyrene-containing analogs can be successfully used as antimicrobial agents.[21]

For such defined substrates, four competitive 32CA reaction paths are possible. They are composed of two regioisomeric pathways, of which each one has two, likely, stereoisomeric pathways.

Complexity of the described process led us to use the computational methods based on molecular electron density theory (MEDT)[22] in order to understand the reaction mechanism and, as a result, make an attempt of synthetic study in a future.

This theoretical research was divided into four parts. First, a topological analysis of electron localization function (ELF)[23] and natural population analysis (NPA)[24,25] for substrates **1** and **2a–c** at the ground state were done. These analyses were presented in order to characterize the electronic structure of the substrates and to predict their reactivity in 32CA reaction based on electron density distribution in molecules.[17] ELF localization domains, ELF basin attractor positions, together with the valence basin populations are shown in Figure 2. The analysis was performed using B3LYP/6-31G(d) theory level in gas phase.

The ELF topological analysis of (*Z*)-1-(anthracen-9-yl)-*N*-methyl nitrone (**1**) shows the presence of two monosynaptic basins, V(O1) and V'(O1), integrating a total electron population of 5.94 e, located at the more nucleophilic O1 atom; one V(O1,N2) disynaptic basin, integrating 1.36 e, associated with an underpopulated O1–N2 single bond; and one V(N2,C3) disynaptic basin, integrating 4.04 e, associated with a N2=C3 double bond (Fig. 2). Due to the absence of pseudoradical center nor a carbenoid center as well as the absence of a double bond, nitrone **1** can be classified as zwitterionic TAC (*zw*-type).[17]

The ELF topology of *trans*-β-nitrostyrene (**2b**) presents one pair of disynaptic basins, V(C4,C5) and V'(C4,C5), integrating a total electron population of 3.52 e. A similar situation is observed both for *trans*-4-amino-β-nitrostyrene (**2a**) and *trans*-4-nitro-β-nitrostyrene (**2c**). The ELF topological analysis of nitrostyrene **2a** shows one pair of disynaptic basins, V(C4,C5) and V'(C4,C5), integrating a total electron population of 3.56 e. In turn, the ELF topology of nitroalkene **2c** shows one pair of disynaptic basins, V(C4,C5) and V'(C4,C5), integrating a total electron population of 3.54 e. The presence of one pair of V(C4,C5) and V'(C4,C5) disynaptic basins is associated with a C4=C5 double bond in nitroalkenes **2a–c** structures (Fig. 2). The presence of V(C4,C5) and V'(C4,C5) basins of *trans*-β-nitrostyrene analogs **2a–c** is associated with a depopulated C4=C5 double bond caused by neighbourhood of groups NO_2 and Ph.

Based on ELF analysis, the proposed Lewis-like structures together with the natural atomic charges for nitrone **1** and nitroalkenes **2a–c** are given in Figure 3.

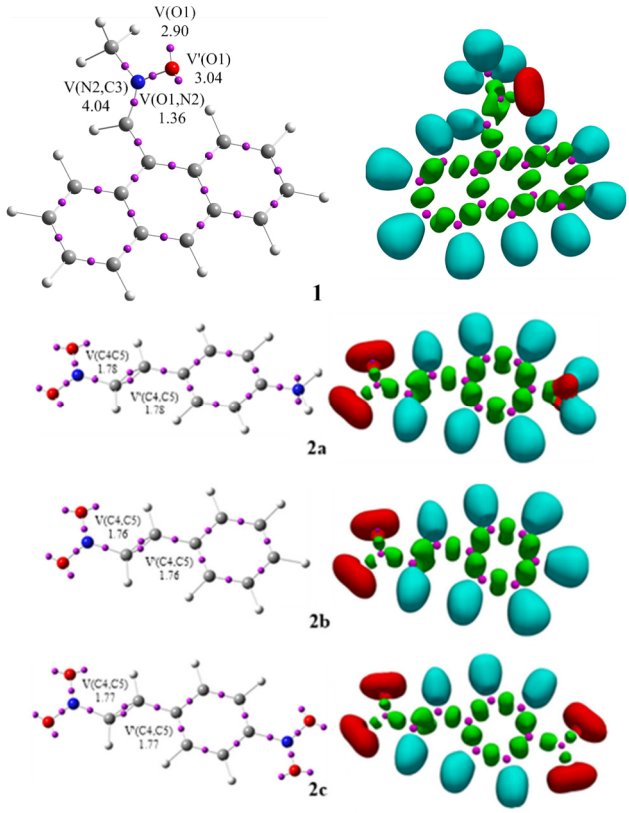

Figure 2. B3LYP/6-31G(d) ELF localization domains of nitrone **1** and nitroalkenes **2a–c** represented at an isosurface value of ELF 0.75 and ELF basin attractor positions, together with the most significant valence basin populations. ELF valence basin populations are given in average number of electrons (e). Protonated basins are shown in blue, monosynaptic basins in red, disynaptic basins in green. The ELF attractors are shown as purple spheres.

While the ELF topological analysis provides a bonding pattern concordant with the commonly accepted Lewis structure, the NPA analysis represents reagents electronic structure. NPA analysis of the natural atomic charges shows that in (*Z*)-1-(anthracen-9-yl)-*N*-methyl nitrone (**1**), the atom O1 is strongly negatively charged by –0.51 e, while the atom N is weakly positive charged by +0.09 e. In turn, C3 carbon presents a formally negligible charge of –0.04 e (Fig. 3). Therefore, NPA indicates that nitrone **1**

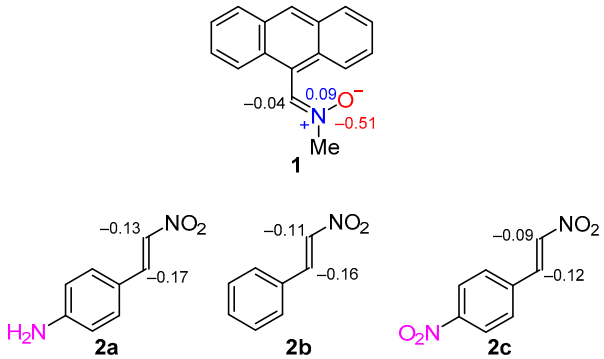

Figure 3. ELF-based Lewis-like structures for nitrone **1** and nitroalkenes **2a–c** proposed by B3LYP/6-31G(d), together with the natural atomic charges. Natural atomic charges are given in average number of electrons (e).

does not possess a 1,2-zwitterionic charge distribution. Presented charge distribution is a consequence of the polarization of the O–N–C framework toward the more electronegative O1 oxygen.

NPA analysis of the natural atomic charges indicates that nitroalkenes **2a–c** show a similar charge distribution. Both ethylene carbons are negatively charged. More electrophilic C_α carbon atoms possess more negative charge compared to C_β carbon atoms. In *trans*-β-nitrostyrene (**2b**), the charge of C_α carbon is –0.16 e, while charge of C_β carbon is –0.11 e. Introduction of electron-donating NH_2 group at *para* position of *trans*-β-nitrostyrene **2a** causes a slight increase of electronic charge distribution of *trans*-4-amino-β-nitrostyrene (**2a**) to –0.17 e (C_α) and –0.13 e (C_β). In turn, in a case of electron-withdrawing NO_2 group electronic charge distribution values of nitroalkene **2c** are reduced to –0.12 e (C_α) and –0.09 e (C_β).

An analysis of the electronic properties of substrates and their intermolecular interactions according to conceptual density functional theory (CDFT)[26,27] reactivity indices was carried out during our theoretical research on 32CA reaction. The global reactivity indices, namely, electronic chemical potential μ,[26] chemical hardness η, global electrophilicity ω, and global nucleophilicity *N*, for the reagents involved in these 32CA reactions were calculated at the B3LYP/6-31G(d) theory level in the gas phase (Table 1).[26,27]

The electronic chemical potential of nitrone **1** (μ –3.50 eV) is higher in comparison to nitroalkenes **2a–c**: μ –3.96 eV (nitroalkene **2a**), –4.79 eV (nitroalkene **2b**) and –5.58 eV (nitroalkene **2c**). It means that the flux of the electron density presumably takes place from (*Z*)-1-(anthracen-9-yl)-*N*-methyl nitrone (**1**) to *trans*-β-nitrostyrene analogs **2a–c**. Thus, discussed 32CA reactions can be classified as the forward electron density flux (FEDF).[28]

Calculated electrophilicity[29] index ω of (*Z*)-1-(anthracen-9-yl)-*N*-methyl nitrone (**1**) is 1.90 eV and the calculated nucleophilicity[30] index *N* for this nitrone **1** is 4.00 eV (Table 1). These values allow to conclude that nitrone **1** can be classified as strong electrophile as well as strong nucleophile in a polar reaction within the electrophilicity and nucleophilicity scale.[26,31]

The calculated electrophilicity index ω of nitroalkene **2b** is 2.66 eV and the calculated nucleophilicity *N* index for this compound is 2.17 eV (Table 1). Thus, *trans*-β-nitrostyrene (**2b**) can be classified as strong electrophile and moderate nucleophile in a polar reaction based on the electrophilicity and nucleophilicity scale.[26]

Introduction of electron-donating group NH_2 at *para* position has a slight impact on the electrophilicity index ω of nitroalkene **2a** with a decrease to 2.17 eV and significant increase of nucleophilicity index *N* to 3.34 eV (Table 1). In consequence, *trans*-4-amino-β-nitrostyrene (**2a**) can be considered a strong electrophile as well as a strong nucleophile.[26]

In turn, introduction of electron-withdrawing group NO_2 significantly increases the electrophilicity index ω of nitroalkene **2c** to 3.70 eV and slightly reduces its nucleophilicity index *N* to 1.44 eV (Table 1). So, *trans*-4-nitro-β-nitrostyrene (**2c**) can be classified as a superelectrophile and marginal nucleophile.[26,31]

Table 1. The global reactivity indices for nitrone **1** and nitroalkenes **2a–c**, calculated based on B3LYP/6-31G(d) theory level in gas phase

Compound	μ, eV	η, eV	ω, eV	*N*, eV
1	–3.50	3.23	1.90	4.00
2a	–3.96	3.62	2.17	3.34
2b	–4.79	4.31	2.66	2.17
2c	–5.58	4.21	3.70	1.44

Overall, for all studied 32CA reactions, it can be assumed that (*Z*)-1-(anthracen-9-yl)-*N*-methyl nitrone (**1**) most evidently can participate as nucleophilic component, while nitroalkenes **2a–c** remain electrophilic substrates. Thus, the regioselectivity of 32CA including the participation of nonsymmetric reagents can be defined through interaction between the most electrophilic center of the electrophile and the most nucleophilic center of the nucleophile.[32] Therefore, in order to characterize the most nucleophilic and the most electrophilic centers of the species involved, the electrophilic P_k^+ and nucleophilic P_k^- Parr functions together with local electrophilicity ω_k and local nucleophilicity N_k of substrates **1** and **2a–c** were analyzed (Fig. 4).[33]

Four different isomeric products can be formed in 32CA reaction between (*Z*)-1-(anthracen-9-yl)-*N*-methyl nitrone (**1**) and *trans*-β-nitrostyrene analogs **2a–c** (Scheme 1).

Analysis of the nucleophilic P_k^- Parr functions of (*Z*)-1-(anthracen-9-yl)-*N*-methyl nitrone (**1**) indicates that O atom of nitrone fragment includes the most nucleophilic center of this species, presenting the maximum value P_O^- 0.22, and the values of the local nucleophilicity index N_k is 0.88 eV (Fig. 4).

The electrophilic P_k^+ Parr functions of *trans*-β-nitrostyrene analogs **2a–c** indicates that C_α atom is the most electrophilic, presenting the maximum value $P_{C\alpha}^+$ 0.29 (nitrostyrene **2a**), 0.25 (nitrostyrene **2b**), and 0.12 (nitrostyrene **2c**) and the values of the local electrophilicity index ω_k are 0.63 (nitrostyrene **2a**), 0.67 (nitrostyrene **2b**), and 0.44 eV (nitrostyrene **2c**, Fig. 4).

So, based on CDFT theory, the most favorable reaction paths are determined by the nucleophilic attack of O atom of (*Z*)-1-(anthracen-9-yl)-*N*-methyl nitrone (**1**) on electrophilic C_α atom of *trans*-β-nitrostyrene analogs **2a–c**. Therefore, the creation of compounds **3a–c** and/or **4a–c** as the most favored regioisomeric adducts is equally probable (Scheme 1).

Further, the kinetic and thermodynamic analysis of potential energy surface (PES) was presented for reaction between (*Z*)-1-(anthracen-9-yl)-*N*-methyl nitrone (**1**) with *trans*-β-nitrostyrene (**2b**) (Table 2). By analogy, the results for reaction of nitrone **1** with the rest of nitroalkenes **2a**,**c** are given in Tables S1 and S2 (Supplementary information file). The computational study was performed using the MPWB95/6-311G(d,p) theory level. The solvent effect was included *via* polarizable continuum model (PCM) for PhMe and EtOH solutions.

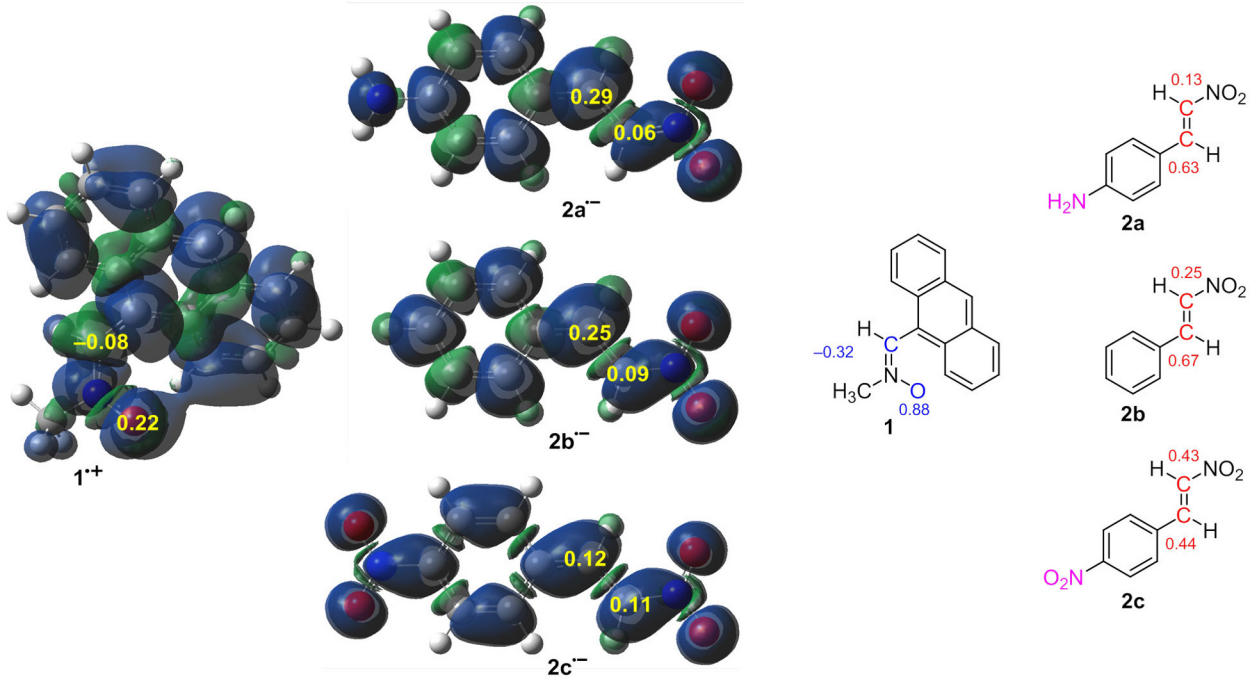

Figure 4. The local electronic properties are presented as 3D models of Mulliken atomic spin densities for nitroalkenes **2a**–**c**$^{\bullet-}$ radical anions and nitrone **1**$^{\bullet+}$ radical cation, together with the electrophilic P_k^+ Parr functions of nitroalkenes **2a**–**c** and the nucleophilic P_k^- Parr functions of nitrone **1** and indices of the local electrophilicity ω_k (eV) of nitroalkenes **2a**–**c**, given in red, and the local nucleophilicity N_k (eV) of nitrone **1**, given in blue.

The analysis of Eyring parameters shows that for the reaction between (*Z*)-1-(anthracen-9-yl)-*N*-methyl nitrone (**1**) and *trans*-β-nitrostyrene (**2b**) in PhMe (ε 2.4) the cycloaddition's enthalpies are negative: –2.76 (**MC$_{3b}$**), –1.65 (**MC$_{4b}$**), –4.84 (**MC$_{5b}$**), –3.25 (**MC$_{6b}$**). This is due to formation of the molecular complex (MC) at the first reaction stage (Table 2, Fig. 5). For all of the possible reaction paths MCs are created without the necessity of crossing an activation barrier. Therefore, MCs may not exist as stable complexes.

Table 2. Kinetic and thermodynamic parameters for 32CA reaction of nitrone **1** with *trans*-β-nitrostyrene (**2b**) in different solvents, according to MPWB95/6-311G(d,p) (PCM) calculations (ΔH and ΔG are given in kcal·mol^{-1}, ΔS is given in cal/(mol·K))*

Reaction step	PhMe (ε 2.4)			EtOH (ε 24.8)		
	ΔH	ΔG	ΔS	ΔH	ΔG	ΔS
1 + **2b** → **MC$_{3b}$**	–2.76	8.85	–38.94	–1.22	13.04	–47.80
1 + **2b** → **TS$_{3b}$**	16.86	32.46	–49.70	23.92	39.48	–52.18
1 + **2b** → **3b**	–0.47	14.35	–52.33	2.37	17.08	–49.33
1 + **2b** → **MC$_{4b}$**	–1.65	10.70	–41.40	–0.31	12.79	–43.94
1 + **2b** → **TS$_{4b}$**	23.62	39.26	–52.45	30.88	46.93	–53.83
1 + **2b** → **4b**	6.19	22.79	–55.69	8.83	25.19	–54.88
1 + **2b** → **MC$_{5b}$**	–4.84	6.35	–37.55	–0.88	11.26	–40.73
1 + **2b** → **TS$_{5b}$**	20.23	34.92	–49.28	27.54	42.97	–51.76
1 + **2b** → **5b**	6.12	22.27	–54.17	8.82	24.75	–53.45
1 + **2b** → **MC$_{6b}$**	–3.25	8.43	–39.19	–1.58	10.12	–39.26
1 + **2b** → **TS$_{6b}$**	18.30	33.57	–51.20	25.54	41.12	–52.27
1 + **2b** → **6b**	1.00	16.99	–53.62	4.21	20.02	–53.00

* MC – molecular complex, TS – transition state, ε – relative permittivity.

Further MC conversion along the reaction proceeds to the transition states (TSs), irrespective to the 32CA pathway. Results of intrinsic reaction coordinate (IRC) analysis indicate the appearance of TSs with the one imaginary eigenvalue in the Hessian. The IRC calculations connect transition state directly with the energy minimum of MC and product in any reaction pathways. It also confirms the absence of more energy minimum connected with the presence of other critical structures. Therefore, we conclude that the mechanism of reaction between (*Z*)-1-(anthracen-9-yl)-*N*-methyl nitrone (**1**) and *trans*-β-nitrostyrene (**2b**) should be considered as one-step. The TSs forming is associated

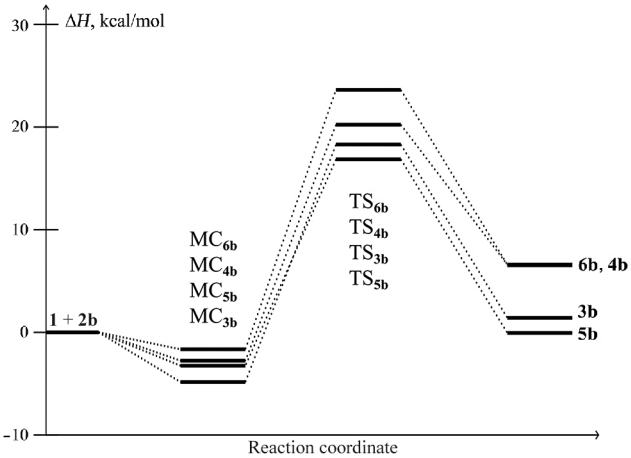

Figure 5. Enthalpy profile for 32CA reaction of (*Z*)-1-(anthracen-9-yl)-*N*-methyl nitrone (**1**) with *trans*-β-nitrostyrene (**2b**) in PhMe, according to MPWB95/6-311G(d,p) (PCM) calculations.

with increase of the Gibbs free energy of the process to 14.35 kcal·mol^{-1} (Table 2, Fig. 5). Data in Table 2 suggests that the forming of (3*RS*,4*RS*,5*SR*)-3-(anthracen-9-yl)-2-methyl-4-nitro-5-phenylisoxazolidine (**3b**) is the most preferable product from the kinetic point of view. The activation barrier in this case is 32.46 kcal·mol^{-1} (Table 2). The obtained results correspond well with the the CDFT analysis results discussed above. In turn, the creation of (3*RS*,4*SR*,5*RS*)-3-(anthracen-9-yl)-2-methyl-4-nitro-5-phenyl-isoxazolidine (**4b**) as the second regioisomer should be considered as unfavorable from the kinetic point of view with the highest activation barrier 39.26 kcal·mol^{-1} (Table 2, Fig. 5). On the other hand, the activation barriers of both regio-isomers **5b** and **6b** are comparable (34.92 and 33.57 kcal·mol^{-1}, respectively) and the formation of these two products is of similar probability under the 32CA conditions in PhMe (Table 2).

In the case of more polar solvent EtOH (ε 24.8), solution is included as dielectric media to DFT calculations as the result the reaction profiles do not change qualitatively, but only quantitatively to a small extent comparing to the results calculated for PhMe solution. In particular, the increase of Δ*H* and Δ*S* values for all MCs are observed as well as activation barriers are significantly higher.[34] Nevertheless, the paths preference of **1** + **2b** reaction based on kinetic aspects for EtOH is identical as in a case of PhMe solution (Table 2).

Finally, the last calculation part includes the diagnostic analysis for all critical structures of the reaction. Similarly to kinetic and thermodynamic studies, the MPWB95/6-311G(d,p) (PCM) theory level was applied for calculation. The results include key parameters[35] such as interatomic distance between reaction centers for significant structures (*r*), development of new single bond (*l*), asymmetry index Δ*l* and the global electron density transfer (GEDT) values and are given in average number of electrons in PhMe (Table 3) and in EtOH (Table 4). Due to similar results, the data for 32CA reactions of methyl nitrone **1** with nitroalkenes **2a**,**c** are given in Tables S3 and S4 (Supplementary information file). The visualisation of key critical structures is shown only for the most favorable **1** + **2b** reaction path leading to oxazolidine **3b** in PhMe solution (Fig. 6).

As noted above, the first stage of 32CA reaction **1** + **2b** in PhMe is the formation of a MC, independently from reaction path (Table 3, Fig. 6). The analysis of the structural aspects shows that within MC distances between reaction centres C3–C4 and C5–O1 remained outside the typical *r* range for bonds in transition state. It can be concluded that in all MCs no new single bonds start forming. GEDT parameters for each MC are equal to 0.0 e, which demonstrates that none of the MC forms electron density transfer complex (Table 3).[36]

The next reaction step is the formation of TS (Table 3, Fig.6). Distances C3–C4 and C5–O1 in the following TS are significantly shortened compared with the corresponding distances within the MC. The nature of TS depends on the relative orientations of complex subunits. In particular, for the **TS$_{3b}$** the extent of C3–C4 and C5–O1 forming new bonds is identical with calculated distances equal to 0.79 and 0.72 Å, respectively (Table 3). In turn, for the same regioisomer but competitive stereoisomer **4b** the predicted **TS$_{4b}$** is more asynchronous. Thus, the distance C3–C4 is *l* 0.78 Å, while C5–O1 predicted bond length is 0.61 Å (Δ*l* 0.17 Å). The two other possible **TS$_{5b}$** and **TS$_{6b}$** are also asynchronous with interatomic distance asymmetry index Δ*l* 0.15 and 0.16 Å, respectively.

Table 3. The key parameters of the critical structures for 32CA reaction of (*Z*)-1-(anthracen-9-yl)-*N*-methyl nitrone (**1**) and *trans*-β-nitrostyrene (**2b**) in PhMe (ε 2.4), according to MPWB95/6-311G(d,p) (PCM) calculations

Structure	C3–C4		C5–O1		Δ*l*, Å	GEDT, e
	r, Å	l_{C3-C4}, Å	*r*, Å	l_{C5-O1}, Å		
MC$_{3b}$	2.884		3.411			0.00
TS$_{3b}$	1.892	0.79	1.891	0.72	0.07	0.19
3b	1.564		1.480			
MC$_{4b}$	2.768		3.436			0.00
TS$_{4b}$	1.936	0.78	1.905	0.61	0.17	0.18
4b	1.585		1.374			
MC$_{5b}$	4.232		3.342			0.00
TS$_{5b}$	2.112	0.67	1.733	0.82	0.15	0.11
5b	1.588		1.469			
MC$_{6b}$	4.003		3.262			0.00
TS$_{6b}$	2.135	0.63	1.779	0.79	0.16	0.14
6b	1.558		1.465			

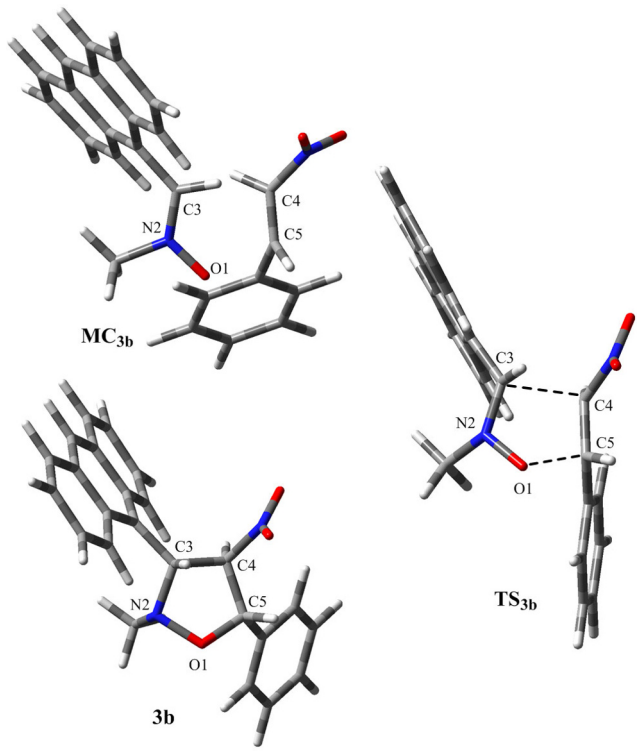

Figure 6. Critical structures for 32CA reaction path of **1** + **2b** → **3b** in PhMe solution according to MPWB95/6-311G(d,p) (PCM) calculations.

Table 4. The key parameters of the critical structures for 32CA reaction of (*Z*)-1-(anthracen-9-yl)-*N*-methyl nitrone (**1**) with *trans*-β-nitrostyrene (**2b**) in EtOH (ε 24.8), according to MPWB95/6-311G(d,p) (PCM) calculations

Structure	C3–C4		C5–O1		Δ*l*, Å	GEDT, e
	r, Å	l_{C3-C4}, Å	*r*, Å	l_{C5-O1}, Å		
MC$_{3b}$	3.244		2.902			0.00
TS$_{3b}$	1.848	0.82	2.080	0.51	0.31	0.26
3b	1.561		1.396			
MC$_{4b}$	2.996		3.489			0.00
TS$_{4b}$	1.850	0.83	1.968	0.57	0.26	0.17
4b	1.584		1.375			
MC$_{5b}$	3.862		3.001			0.00
TS$_{5b}$	2.139	0.66	1.665	0.88	0.22	0.19
5b	1.590		1.474			
MC$_{6b}$	4.031		3.291			0.00
TS$_{6b}$	2.164	0.62	1.702	0.84	0.22	0.22
6b	1.566		1.464			

So, during the most kinetically favored reaction pathway, the formation of synchronic transition state is also more favorable. Noteworthy, that all TSs calculated for PhMe exhibit low polar nature in the range of GEDT 0.11–0.19 e (low polar GEDT parameter 0.05 < GEDT < 0.20, Table 3).[30] However, the most preferred reaction pathway **1** + **2b** → **3b** in EtOH is characterized by GEDT 0.26 e and by the most synchronous **TS$_{3b}$** (Table 4).[37]

The value changes of key parameters of the transformation in EtOH is only quantitative. Preferences regarding the length of interatomic distances, single bond development indices as well as synchronicity and polarity character of reactions are similar to those calculated for PhMe (Table 4). Still, in all of TSs in EtOH an increase of asynchronicity degree as well as the increase of the GEDT values can be observed, which is due to the more polar nature of the solvent.

To sum up, the presented quantum-chemical studies of [3+2] cycloaddition reactions between (*Z*)-1-(anthracen-9-yl)-*N*-methyl nitrone and *trans*-β-nitrostyrene analogs clearly indicate to a one-step asynchronous mechanism. The polar character of processes depends on the type of simulated solvent. The presented ELF and CDFT calculations show that the most favorable reaction path is determined by the nucleophilic attack of atom O of nitrone on the electrophilic C_α atom of nitroalkenes. Accordingly, the formation of regioisomer of 3-(anthracen-9-yl)-5-aryl-2-methyl-4-nitroisoxazolidine is the most probable. In turn, the analysis of kinetic and thermodynamic parameters as well as the diagnosis of critical structures for studied [3+2] cycloaddition reactions confirms the previous regioisomeric preference, and demonstrates the formation of (3*RS*,4*RS*,5*SR*)-3-(anthracen-9-yl)-5-aryl-2-methyl-4-nitroisoxazolidine as the most probable product among all possible.

Computational details

The calculations associated with the [3+2] cycloaddition reactions were performed using the Gaussian 09 package[38] at the Prometheus computer cluster of the CYFRONET regional computational center in Cracow. DFT calculations were performed using the MPWB95/6-311g(d,p)[39] theory level. The similar computational level has already been successfully used for the exploration of mechanistic aspects of different cycloaddition processes.[40–43] Calculations of critical structures were performed at 298K temperature and 1 atm pressure. The localized stationary points were characterized using vibrational analysis. For optimized TS, intrinsic reaction coordinate (IRC)[44] calculations have been performed to verify whether the located TSs are connected to the corresponding minimum stationary points associated with reactants and products.

The solvent effects were simulated using a standard self-consistent reaction field (SCRF)[45,46] based on the polarizable continuum model (PCM).[47]

The global electron density transfer (GEDT)[37] values were estimated by the natural population analysis (NPA)[24,25] using the equation GEDT(*f*) = charge q_f, where *q* are the atoms of a framework (*f*) of the TSs.

Indices of single bond development (*l*) were calculated according to the formula:[48]

$$l_{X-Y} = 1 - \frac{r^{TS}_{X-Y} - r^{P}_{X-Y}}{r^{P}_{X-Y}}$$

where $r_{X-Y}{}^{TS}$ is the distance between the reaction centers X and Y in the transition structure and $r_{X-Y}{}^{P}$ is the same distance in the corresponding product.

Global electronic properties of the reactants were estimated according to the equations recommended in references.[49] The CDFT indices were calculated at the B3LYP/6-31G(d) computational level in gas phase also used to define the electrophilicity and nucleophilicity scales.[26,31,50] Electrophilic P_k^+ and nucleophilic P_k^- Parr functions were obtained from the changes of atomic spin density (ASD) of the reagents.[33,50]

Topological analysis of the electron localization function (ELF)[23] was performed with the TopMod[51] program, using monodeterminantal wave functions over a grid spacing of 0.1 au. Calculation was performed on B3LYP/6-31G(d) level theory in gas phase.

GaussView program[52] was used to visualize molecular geometries and 3D representations of the radical anion and the radical cations and the position of the ELF basin attractors. The ELF localization domains at an isovalue of 0.75 au were obtained with the Paraview software.[53,54]

Supplementary information file, containing the kinetic and thermodynamic data as well as the key parameters of the critical structures for the 32CA reactions **1** + **2a** and **1** + **2c**, and cartesian coordinates of critical key structures is available at the journal website http://link.springer.com/journal/10593.

This work was partially supported by PLGrid Infrastructure.

All calculations reported in this paper were performed on Prometheus supercomputer cluster in the CYFRONET computational center in Cracow.

References

1. Fryźlewicz, A.; Łapczuk-Krygier, A.; Kula, K.; Demchuk, O. M.; Dresler, E.; Jasiński, R. *Chem. Heterocycl. Compd.* **2020**, *56*, 120.
2. Lakhvich, F. A.; Koroleva, E. V.; Akhrem, A. A. *Chem. Heterocycl. Compd.* **1989**, *25*, 359.
3. Rescifina, A.; Chiacchio, M. A.; Corsaro, A.; De Clercq, E.; Ianuazzo, D.; Mastino, A.; Piperno, A.; Romeo, G.; Romeo, R.; Valveri, V. *J. Med. Chem.* **2006**, *49*, 709.
4. Mochulskaya, N. N.; Nosova, E. V.; Charushin, V. N. *Chem. Heterocycl. Compd.* **2021**, *57*, 374.
5. Mirzayev, F.; Viney, K.; Linh, N. N.; Gonzalez-Angulo, L.; Gegia, M.; Jaramillo, E.; Zignol, M.; Kasaeva, T. *Eur. Respir. J.* **2021**, *57*, 2003300.
6. Landeck, H.; Ranke, G. US Patent 5413627A.
7. Vretik, L.; Ritter, H. *Macromolecules* **2003**, *36*, 6340.
8. Sirotkina, E. V.; Efremova, M. M.; Starova, G. L.; Kuznetsov, M. A.; Molchanov, A. P. *Chem. Heterocycl. Compd.* **2020**, *56*, 1193.
9. Jasiński, R. *Chem. Heterocycl. Compd.* **2009**, *45*, 748.
10. Markitanov, Y. N.; Timoshenko, V. M. *Chem. Heterocycl. Compd.* **2021**, *57*, 1149.
11. Padwa, A.; Bur, S. *Chem. Heterocycl. Compd.* **2016**, *52*, 616.
12. Kula, K.; Dobosz, J.; Jasiński, R.; Kącka-Zych, A.; Łapczuk-Krygier, A.; Mirosław, B.; Demchuk, O. M. *J. Mol. Struct.* **2020**, *1203*, 127473.
13. Xiang, J.; Zhu, T.; Dang, Q.; Bai, X. *Chem. Heterocycl. Compd.* **2016**, *52*, 601.
14. Kula, K.; Kącka-Zych, A.; Łapczuk-Krygier, A.; Wzorek, Z.; Nowak, A.; Jasiński, R. *Molecules* **2021**, *26*, 1364.
15. Martina, K.; Tagliapietra, S.; Veselov, V. V.; Cravotto, G. *Front. Chem.* **2019**, *7*, 95.
16. Żmigrodzka, M.; Sadowski, M.; Kras, J.; Dresler, E.; Demchuk, O. M.; Kula, K. *Sci. Rad.* **2022**, *1*, 24.
17. Ríos-Gutiérrez, M.; Domingo, L. R. *Eur. J. Org. Chem.* **2019**, *2*, 267.
18. Kula, K.; Dresler, E.; Demchuk, O. M.; Jasiński, R. *Przem. Chem.* **2015**, *94*, 1385.
19. Łapczuk-Krygier, A.; Kącka-Zych, A.; Kula, K. *Curr. Chem. Lett.* **2019**, *8*, 13.
20. Shvekhgeimer, G. A.; Zvolinskii, V. I.; Kobrakov, K. I. *Chem. Heterocycl. Compd.* **1986**, *22*, 353.
21. Boguszewska-Czubara, A.; Kula, K.; Wnorowski, A.; Biernasiuk, A.; Popiołek, Ł.; Miodowski, D.; Demchuk, O. M.; Jasiński, R. *Saudi Pharm. J.* **2019**, *27*, 593.
22. Domingo, L. R. *Molecules* **2016**, *21*, 1319.
23. Becke, A. D.; Edgecombe, K. E. *J. Chem. Phys.* **1990**, *92*, 5397.
24. Reed, A. E.; Weinstock, R. B.; Weinhold, F. *J. Chem. Phys.* **1985**, *83*, 735.
25. Reed, A. E.; Curtiss, L. A.; Weinhold, F. *Chem. Rev.* **1988**, *88*, 899.
26. Domingo, L. R.; Ríos-Gutiérrez, M.; Pérez, P. *Molecules* **2016**, *21*, 748.
27. Parr, R. G.; Yang, W. *Density Functional Theory of Atoms and Molecules*; Oxford University Press: New York, 1989.
28. Domingo, L. R.; Kula, K.; Ríos-Gutiérrez, M.; Jasiński, R. *J. Org. Chem.* **2021**, *86*, 12644.
29. Parr, R. G.; Szentpaly, L. V.; Liu, S. *J. Am. Chem. Soc.* **1999**, *121*, 1922.
30. Domingo, L. R.; Chamorro, E.; Pérez, P. *J. Org. Chem.* **2008**, *73*, 4615.
31. Domingo, L. R.; Ríos-Gutiérrez, M. In *Conceptual Density Functional Theory: Towards a New Chemical Reactivity Theory*; Liu, S., Ed.; WILEY-VCH GmbH: Weinheim, 2022, vol. 2, p. 481.
32. Aurell, M. J.; Domingo, L. R.; Pérez, P.; Contreras, R. *Tetrahedron* **2004**, *60*, 11503.
33. Domingo, L. R.; Pérez, P.; Sáez, J. A. *RSC Adv.* **2013**, *3*, 1486.
34. Benchouk, W.; Mekelleche, S. M.; Silvi, B.; Aurell, M. J.; Domingo, L. R. *J. Phys. Org. Chem.* **2011**, *24*, 611.
35. Jasiński, R. *Chem. Heterocycl. Compd.* **2022**, *58*, 260.
36. Domingo, L. R.; Ríos-Gutiérrez, M. *Org. Biomol. Chem.* **2019**, *17*, 6478.
37. Domingo, L. R. *RSC Adv.* **2014**, *4*, 32415.
38. Frisch, M. J.; Trucks, G. W.; Schlegel, H. B.; Scuseria, G. E.; Robb, M. A.; Cheeseman, J. R.; Scalmani, G.; Barone, V.; Petersson, G. A.; Nakatsuji, H.; Li, X.; Caricato, M.; Marenich, A.; Bloino, J.; Janesko, B. G.; Gomperts, R.; Mennucci, B.; Hratchian, H. P.; Ortiz, J. V.; Izmaylov, A. F.; Sonnenberg, J. L.; Williams-Young, D.; Ding, F.; Lipparini, F.; Egidi, F.; Goings, J.; Peng, B.; Petrone, A.; Henderson, T.; Ranasinghe, D.; Zakrzewski, V. G.; Gao, J.; Rega, N.; Zheng, G.; Liang, W.; Hada, M.; Ehara, M.; Toyota, K.; Fukuda, R.; Hasegawa, J.; Ishida, M.; Nakajima, T.; Honda, Y.; Kitao, O.; Nakai, H.; Vreven, T.; Throssell, K.; Montgomery, J. A., Jr.; Peralta, J. E.; Ogliaro, F.; Bearpark, M.; Heyd, J. J.; Brothers, E.; Kudin, K. N.; Staroverov, V. N.; Keith, T.; Kobayashi, R.; Normand, J.; Raghavachari, K.; Rendell, A.; Burant, J. C.; Iyengar, S. S.; Tomasi, J.; Cossi, M.; Millam, J. M.; Klene, M.; Adamo, C.; Cammi, R.; Ochterski, J. W.; Martin, R. L.; Morokuma, K.; Farkas, O.; Foresman, J. B.; Fox, D. J. *Gaussian 09*, *Revision D.01*; Gaussian, Inc.: Wallingford, 2013.
39. Zhao, Y.; Truhlar, G. D. *J. Phys. Chem. A* **2004**, *108*, 6908.
40. Zawadzińska, K.; Ríos-Gutiérrez, M.; Kula, K.; Woliński, P.; Mirosław, B.; Krawczyk, T.; Jasiński, R. *Molecules* **2021**, *26*, 6774.
41. Kula, K.; Kącka-Zych, A.; Łapczuk-Krygier, A.; Jasiński, R. *Pure Appl. Chem.* **2021**, *93*, 427.
42. Kula, K.; Łapczuk-Krygier, A. *Curr. Chem. Lett.* **2018**, *7*, 27.
43. Demchuk, O. M.; Jasinski, R.; Strzelecka, D.; Dziuba, K.; Kula, K.; Chrzanowski, J.; Krasowska, D. *Pure Appl. Chem.* **2018**, *90*, 49.
44. Fukui, K. *J. Phys. Chem.* **1970**, *74*, 4161.
45. Tapia, O. *J. Math. Chem.* **1992**, *10*, 131.
46. Tomasi, J.; Perisco, M. *Chem. Rev.* **1994**, *94*, 2027.
47. Cossi, M.; Barone, V.; Cammi, R.; Tomasi, J. *Chem. Phys. Lett.* **1996**, *225*, 327.
48. Mlostoń, G.; Jasiński, R.; Kula, K.; Heimgartner, H. *Eur. J. Org. Chem.* **2020**, *2*, 176.
49. Kula, K.; Zawadzińska, K. *Curr. Chem. Lett.* **2021**, *10*, 9.
50. Mlostoń, G.; Kula, K.; Jasiński, R. *Molecules* **2021**, *26*, 5562.
51. Noury, S.; Krokidis, X.; Fuster, F.; Silvi, B. *Comput. Chem.* **1999**, *23*, 597.
52. Dennington, R.; Keith, T. A.; Millam, J. M. *GaussView*, *Version 6.*; Semichem, Inc.: Shawnee Mission, 2016.
53. Ahrens, J.; Geveci, B.; Law, C. In *ParaView*: *An End-User Tool for Larga Data Visualization. The Visualization Handbook*; Elsevier: Amsterdam, 2005.
54. Ayachit, U. *The ParaView Guide: A Parallel Visualization Application*; Kitware: New York, 2015.